Electronic Supplementary Material (ESI) for ChemComm.

2D amorphous bi-metallic NiFe nitrides for high-efficiency oxygen evolution reaction

Yifan Xu,[a] Zhenfeng Cheng, [a] Jingyun Jiang,*[a] Jiang Du,[a] and Qun Xu*[a,b]

[a]School of Materials Science and Engineering, Zhengzhou University, Zhengzhou, 450001, Henan, China

[b]Henan Institute of Advanced Technology, Zhengzhou University, Zhengzhou, 450052, Henan, China

*Corresponding author E-mail: qunxu@zzu.edu.cn, jiangjingyun@zzu.edu.cn

Table of contents

Table S1 OER performance of NiFe-N-CP and other representative reported non-precious metal electrocatalysts in similar alkaline media.

3. References

1. Experimental Section

1.1 Chemicals and Materials

Polyethylene glycol (PEG) 200, barbituric acid (BA), ferric trichloride hexahydrate ($FeCl_3 \cdot 9H_2O$, ≥ 99%), nickel trichloride hexahydrate ($NiCl_2 \cdot 6H_2O$, ≥ 99%), and absolute ethanol were purchased from Sinopharm Chemical Reagent Co., Ltd. Potassium hydroxide (KOH, ≥ 85%) was purchased from Shanghai Aladdin Biochemical Technology Co. Ltd. Carbon paper (CP) was purchased from Toray Industries Co. Ltd. All chemicals were used directly without further purification. Ultrapure water of 18.2 MΩ cm was used in all experiments.

1.2 Fabrication of samples

Preparation of ternary deep eutectic solvents:

Ternary DESs were synthesized by simple mixing of PEG 200, BA with $MCl_x \cdot yH_2O$ at molar ratios of 16:1:1. Noted that the total number of moles of hydrated Ni/Fe chloride remained consistent during the synthesis of each DES. The detailed synthesized process is shown as follows:

Ternary deep eutectic solvents	Molar Ratio			
	PEG	BA	$MCl_x \cdot yH_2O$	
			$NiCl_2 \cdot 6H_2O$	$FeCl_3 \cdot 9H_2O$
PEG200-BA-$NiCl_2 \cdot 6H_2O$	16	1	1	0
PEG200-BA-$FeCl_3 \cdot 9H_2O$	16	1	0	1
PEG200-BA-$NiCl_2 \cdot 6H_2O$/$FeCl_3 \cdot 9H_2O$-1	16	1	0.990	0.010
PEG200-BA-$NiCl_2 \cdot 6H_2O$/$FeCl_3 \cdot 9H_2O$-2	16	1	0.952	0.048
PEG200-BA-$NiCl_2 \cdot 6H_2O$/$FeCl_3 \cdot 9H_2O$-3	16	1	0.908	0.092
PEG200-BA-$NiCl_2 \cdot 6H_2O$/$FeCl_3 \cdot 9H_2O$-4	16	1	0.834	0.166

Synthesis of 2D Ni-N-CP: 2D Ni-N-CP was synthesized via a one-step eutectic-solvothermal method. In a typically synthesis, 30 mL PEG200-BA-$NiCl_2 \cdot 6H_2O$ DES were transferred into 100 mL Teflon-lined autoclave with 10 pieces fixed CP (1 cm X 1 cm). After reaction at 200

^{o}C for 2 h and cooling down of the autoclave naturally, the CP were collected and cleaned with ultrapure water and ethanol several times, and then dried at 60 ^{o}C in oven.

Synthesis of 2D Fe-N-CP: 2D Fe-N-CP was synthesized the same method of 2D Ni-N-CP except that the DES was changed to PEG200-BA-$FeCl_3 \cdot 9H_2O$.

Synthesis of 2D $NiFe_{0.01}$-N-CP: 2D Fe-N-CP was synthesized the same method of 2D Ni-N-CP except that DES was changed to PEG200-BA-$NiCl_2 \cdot 6H_2O$/$FeCl_3 \cdot 9H_2O$-1.

Synthesis of 2D $NiFe_{0.05}$-N-CP: 2D Fe-N-CP was synthesized the same method of 2D Ni-N-CP except that DES was changed to PEG200-BA-$NiCl_2 \cdot 6H_2O$/$FeCl_3 \cdot 9H_2O$-2.

Synthesis of 2D $NiFe_{0.1}$-N-CP: 2D Fe-N-CP was synthesized the same method of 2D Ni-N-CP except that DES was changed to PEG200-BA-$NiCl_2 \cdot 6H_2O$/$FeCl_3 \cdot 9H_2O$-3.

Synthesis of 2D $NiFe_{0.2}$-N-CP: 2D Fe-N-CP was synthesized the same method of 2D Ni-N-CP except that DES was changed to PEG200-BA-$NiCl_2 \cdot 6H_2O$/$FeCl_3 \cdot 9H_2O$-4.

1.2 Characterization

Differential scanning calorimetry (DSC) was performed using a DSC204 (Netzsch, Germany) system at a heating rate of 5 °C min^{-1}. The Fourier transform-infrared spectroscopy (FT-IR) spectra were conducted on a FT-IR spectrometer (Prestige 21, Shimadzu, Japan, DTGS detector) in a KBr pellet, ranging from 700 to 4000 cm^{-1}.

Scanning electron microscope (SEM) and corresponding energy dispersive X-ray spectroscopy (EDS) experiments were carried out on a SU8010 field scanning electron microscope (Hitachi High-technologies Corporation, Japan) equipped with energy dispersive x-ray spectroscopy at an accelerating voltage of 5 keV.

Transmission electron microscope (TEM), high-resolution TEM (HRTEM) and corresponding EDS mapping measurements were carried out on a FEI Talos F200S TEM (Thermo Fisher Scientific, USA) equipped with EDS with a field emission gun operating at 200 kV. Atomic force microscopy (AFM) experiments were performed on Bruker Dimension ICON. In the TEM and AFM test, samples were obtained by ultrasound from the in-situ NiFe-N-CP electrode.

X-ray powder diffraction (XRD) experiments were performed on Y-2000 X-ray diffractometer (λ = 1.5406 Å) with Cu K radiation at a scanning rate of 10^{o} min^{-1}. The X-ray

photoelectron spectroscopy (XPS) experiments were performed with an XPS, ESCA Lab250 X-ray photoelectron spectrometer (Thermo Fisher Scientific, USA) with Al Kα source. All XPS data were aligned using C 1s line at 284.8 eV fitted according to the smart fitting method

1.4 Electrochemical measurement

All electrochemical measurements were carried out on CHI 760E electrochemical workstation (ChenHua Instrument, Shanghai, China) with a typical three-electrode system in 1 M KOH solution. The Pt gauze electrode and Ag/AgCl electrode were used as the counter electrode and reference electrode, respectively. All the measured potentials were calibrated against the reversible hydrogen electrode (RHE) using the following equation:

$$E_{RHE} = E_{Ag/AgCl} + 0.197 + 0.059*pH$$

The linear sweep voltammogram (LSV) curves were tested at a scan rate of 5 mV s^{-1} in 1 M KOH at room temperature. The Tafel slopes were also derived from the polarization curves. The collected polarization curves shown in the article were calibrated after 90% *iR* correction.

Cyclic voltammogram (CV) curves were tested from -0.05 to 0.05 V (vs. Ag/AgCl) at different scan rates. Electrochemical impedance spectroscopy (EIS) was measured in the potentiostatic mode from 0.1 Hz to 100 kHz. The intrinsic resistance of electrode and electrolyte (R_s), the charge-transfer resistance (R_{ct}) in parallel with the constant phase element (CPE), the EIS spectra are analyzed using the complex nonlinear least-squares fitting method. The multipotential step chronopotentiometry of $NiFe_{0.05}$-N-CP was started at 0.55 V and ended at 0.7 V, with an increment of 0.25 V per step without *iR* correction. Chronopotentiometry of $NiFe_{0.05}$-N-CP at a current density of 22 mA cm^{-2} without *iR* correction.

1.5 Theoretical calculations

The present first-principles calculation was used to investigate the properties in graphene surface structures based on density functional theory (DFT). The Perdew-Burke-Ernzerhof (PBE) with projector-augmented wave (PAW) had been employed in our calculation. It is noted that the 2×2×1 K-points and 400 eV of cut-off energy was used to optimize the surface structure. For our structure, the convergence criterion can be described as: the self-consistent force is less than 10^{-2} eV $Å^{-1}$ and the difference of energy is less than 10^{-6} eV. The Van der Waals has been considered in

the calculation. In addition, for the metal atoms, the U schemes need to be applied, and the U has been set as 1.5 eV. What's more, adsorption molecule, which is considered as fixed molecule, migration barrier energies had been evaluated using the Transition state methods. In our calculation, the binding energy (E_b) can be obtained by the following equation:

$$E_b = E_{total} - E_1 - E_{molecule}$$

where the E_{total} is the surface with molecule adsorbed, E_1 is the energy of the surface, and $E_{molecule}$ is the energy of molecule.

2. Supplementary Figures and Tables

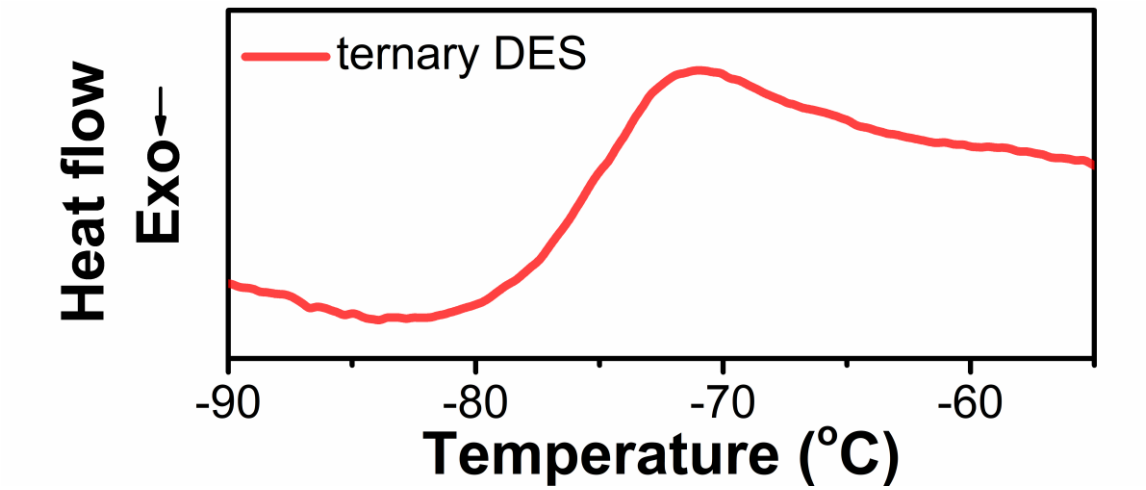

Fig.S1 DSC of ternary DES (PEG200-BA-$NiCl_2 \cdot 6H_2O$/$FeCl_3 \cdot 9H_2O$-2)

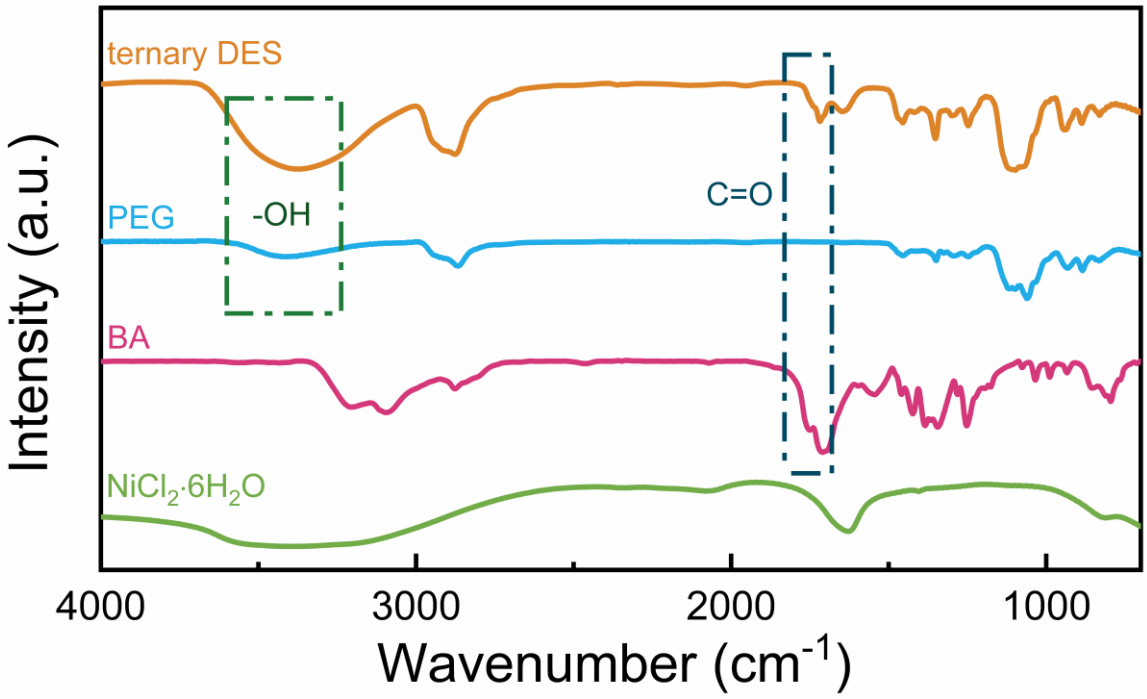

Fig.S2 FT-IR spectrogram of rernary DES, PEG, BA and $NiCl_2{\cdot}6H_2O$

As Fig S2 depicts, C=O peaks are derived from BA shift from 1702 cm^{-1} for pure BA to 1720 cm^{-1} for $NiCl_2{\cdot}6H_2O$-BA-PEG. In addition, -OH peaks are derived from PEG 200 shift from 3406 cm^{-1} for pure PEG to 3370 cm^{-1} for $NiCl_2{\cdot}6H_2O$-BA-PEG, with the half peak widths increase in $NiCl_2{\cdot}6H_2O$-BA-PEG. Such observations indicate that both -OH group and Cl^- alters the surrounding environment of C=O, most likely caused by the formation of H bonds.

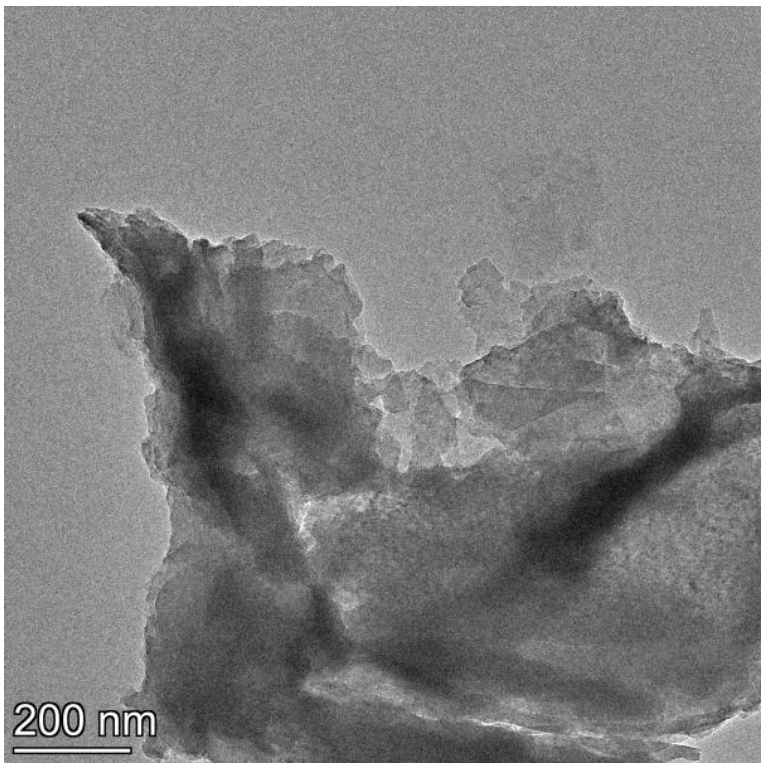

Fig. S3 TEM image of Ni-N.

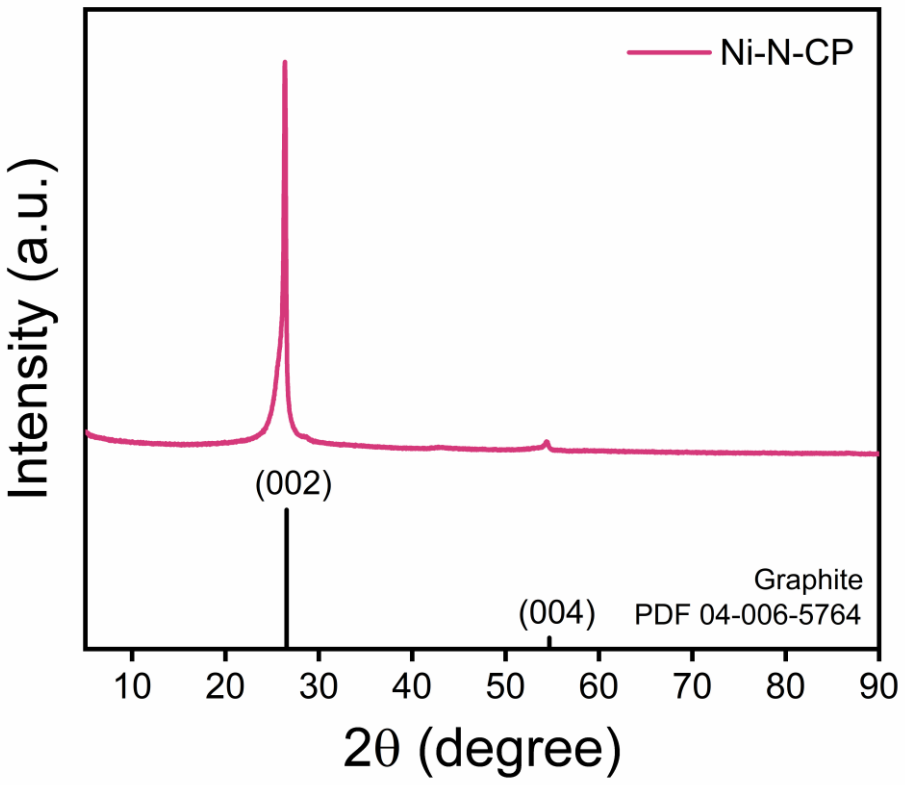

Fig. S4 XRD pattern of Ni-N-CP.

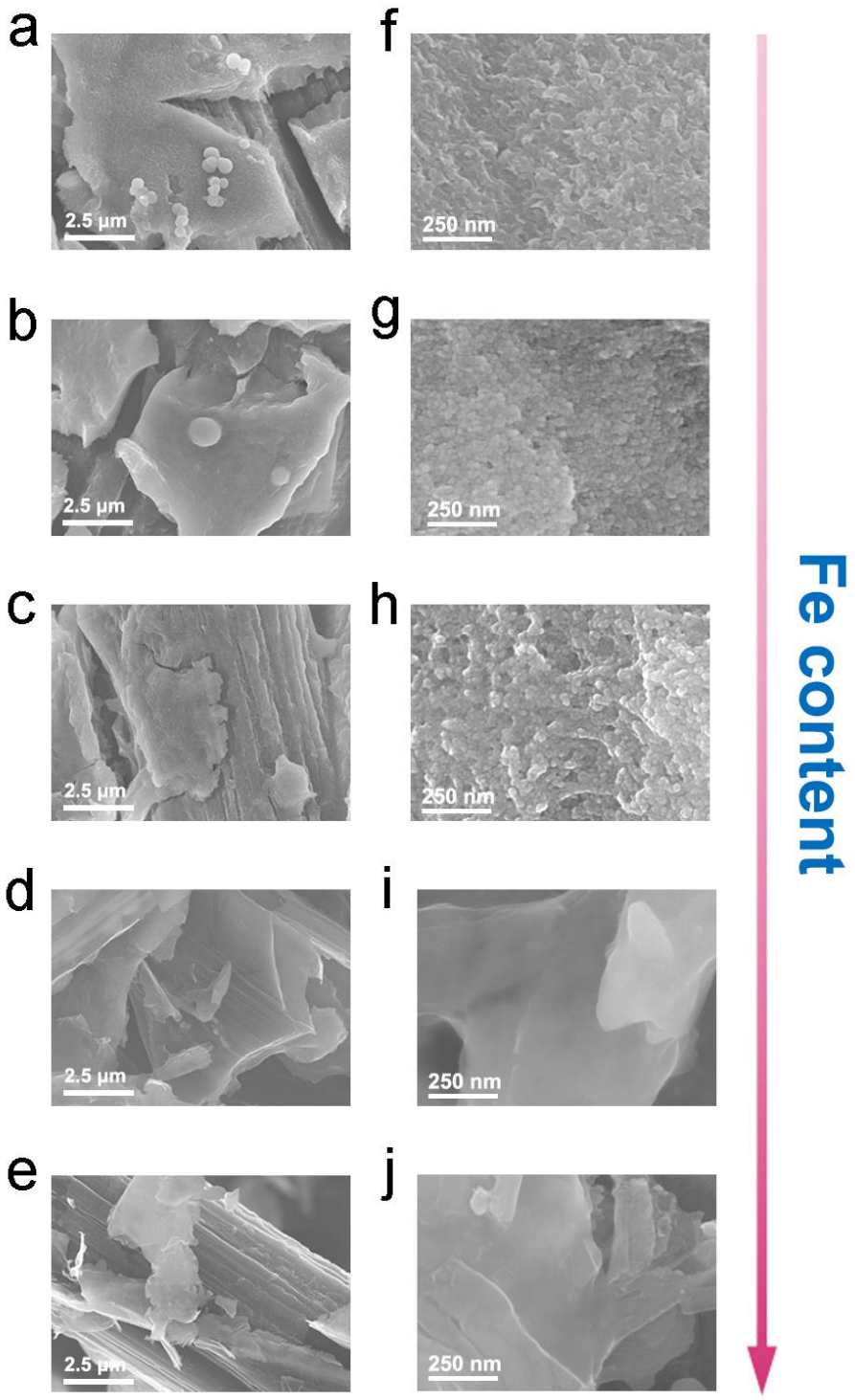

Fig. S5 SEM images of Ni-N-CP (a,f), $NiFe_{0.01}$-N-CP (b,g), $NiFe_{0.05}$-N-CP (c,h), $NiFe_{0.1}$-N-CP (d,i) and $NiFe_{0.2}$-N-CP (e,j).

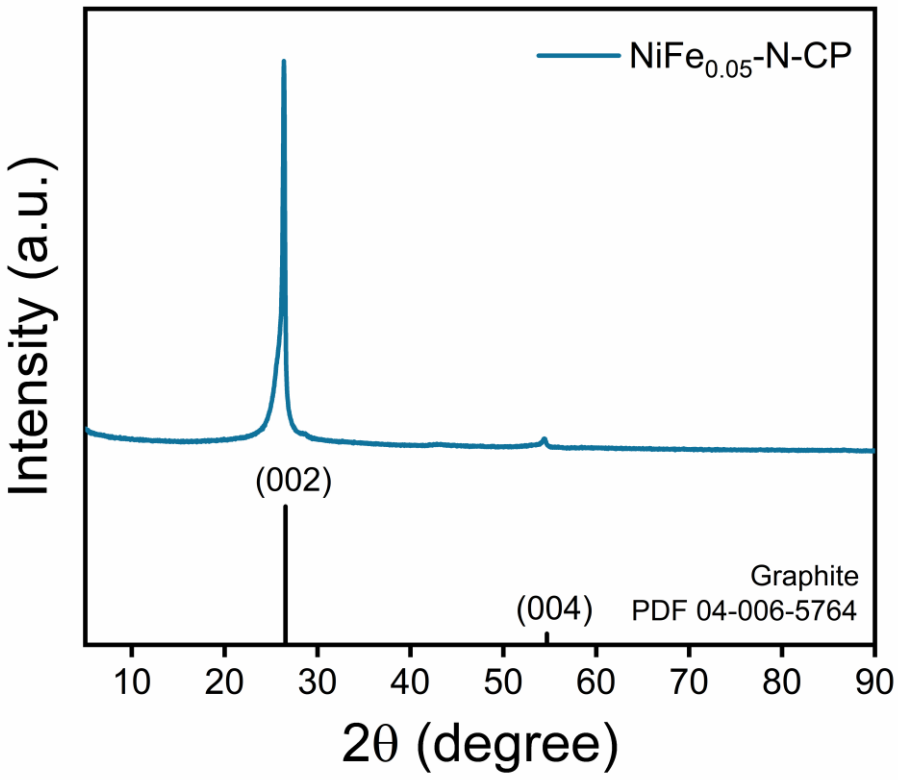

Fig. S6 XRD pattern of $NiFe_{0.05}$-N-CP.

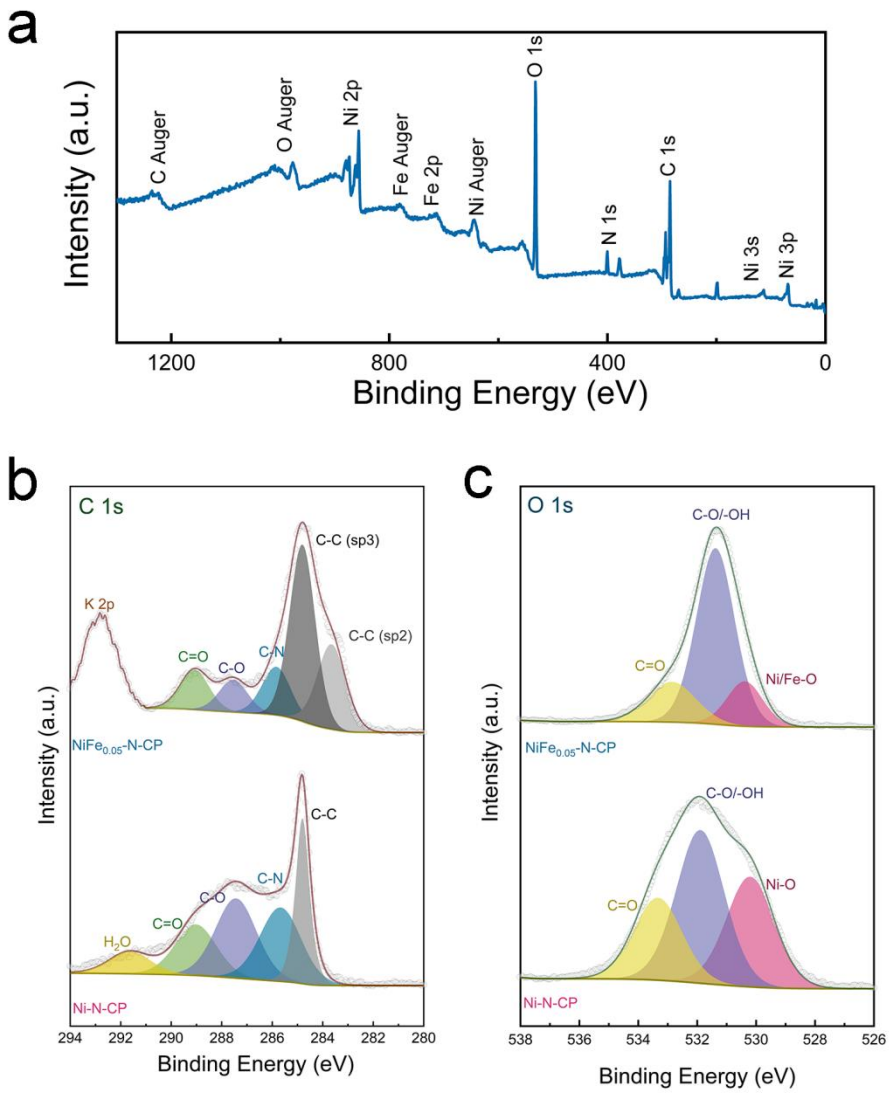

Fig. S7 a) The full XPS survey spectra of $NiFe_{0.05}$-N-CP; (b-c) High-resolution XPS spectra of $NiFe_{0.05}$-N-CP: b) C 1s and c) O 1s.

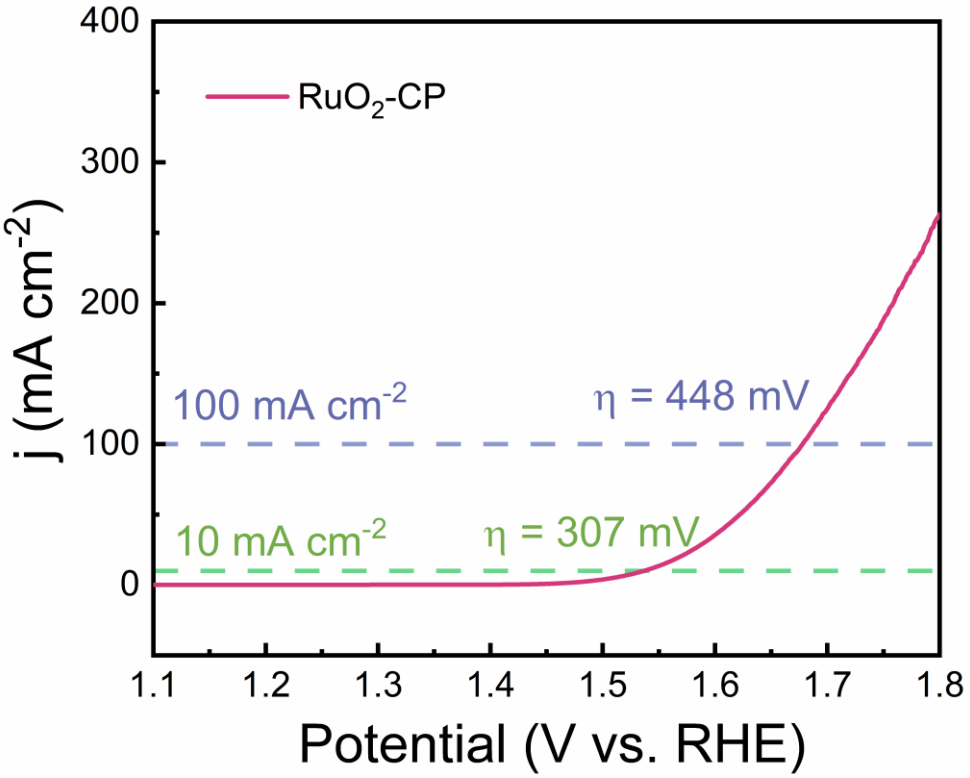

Fig. S8 OER polarization curves of RuO_2-CP.

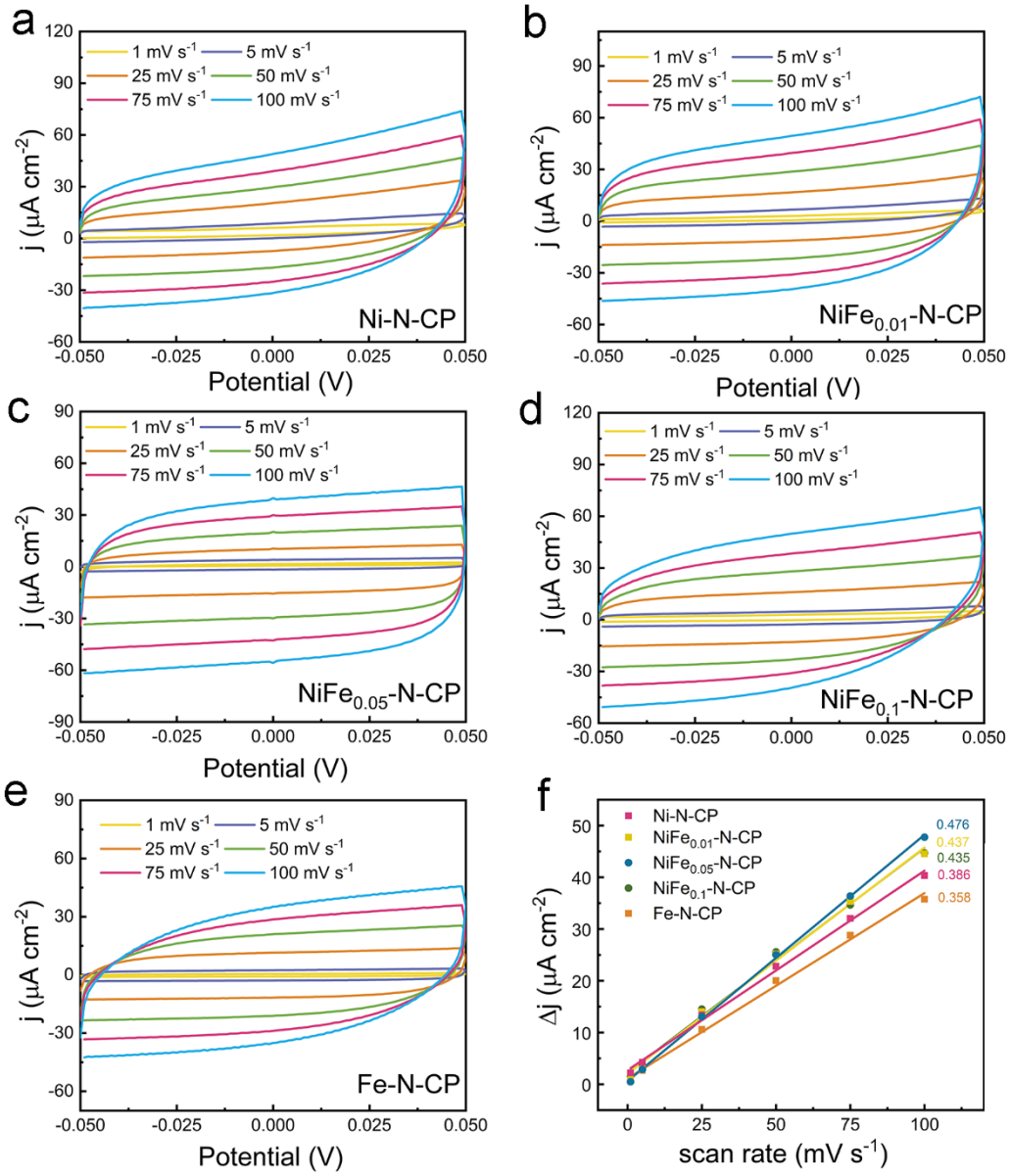

Fig. S9 Cyclic voltammograms of Fe-N-CP (a), Ni-N-CP (b), $NiFe_{0.01}$-N-CP (c), $NiFe_{0.05}$-N-CP (d), and $NiFe_{0.1}$-N-CP (e) in potential from -0.05-0.05V (*vs.* Ag/AgCl) at a class of scan rates of 1, 5, 25, 50, 75, and 100 mV·dec^{-1}; (e) Linear fitting of the oxidation currents of the catalysts at 0 V (*vs.* Ag/AgCl) versus scan rates.

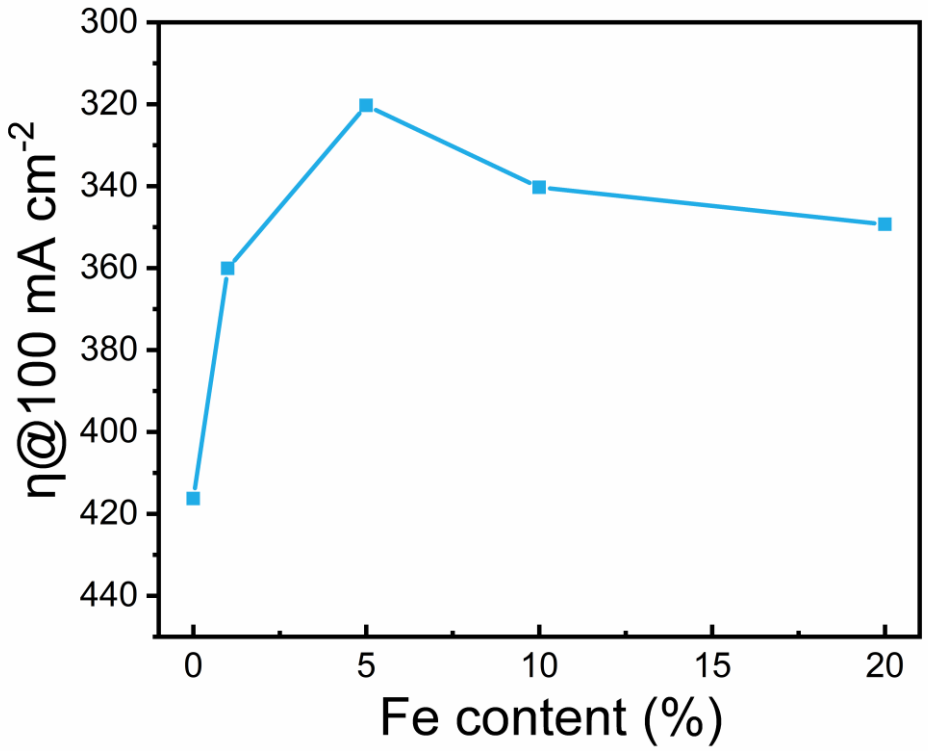

Fig. S10 Overpotentials of $NiFe_X$-N (x = 0, 0.01 ,0.05, 0.1, 0.2) at 100 mA cm^{-2}.

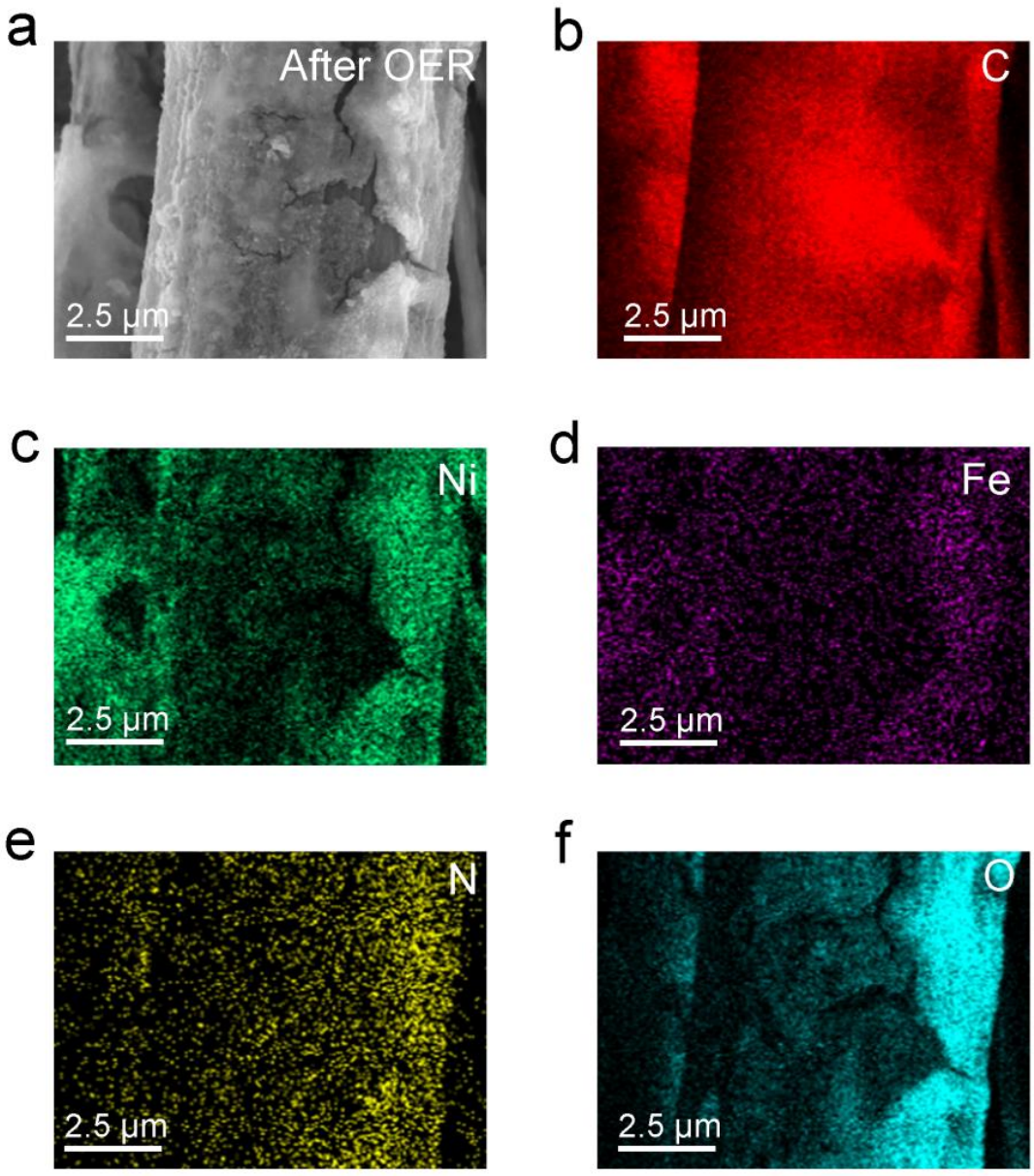

Fig. S11 EDS mapping of $NiFe_{0.05}$-N-CP after the chronopotentiometry for 24 hours.

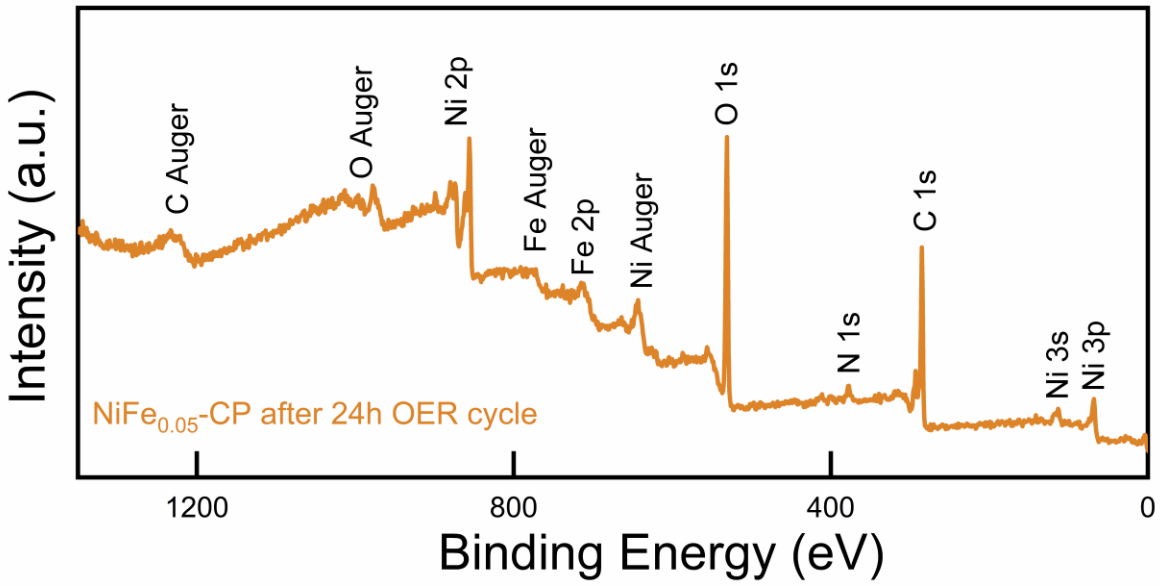

Fig. 12 The full XPS survey spectra of $NiFe_{0.05}$-N-CP after24h OER cycling.

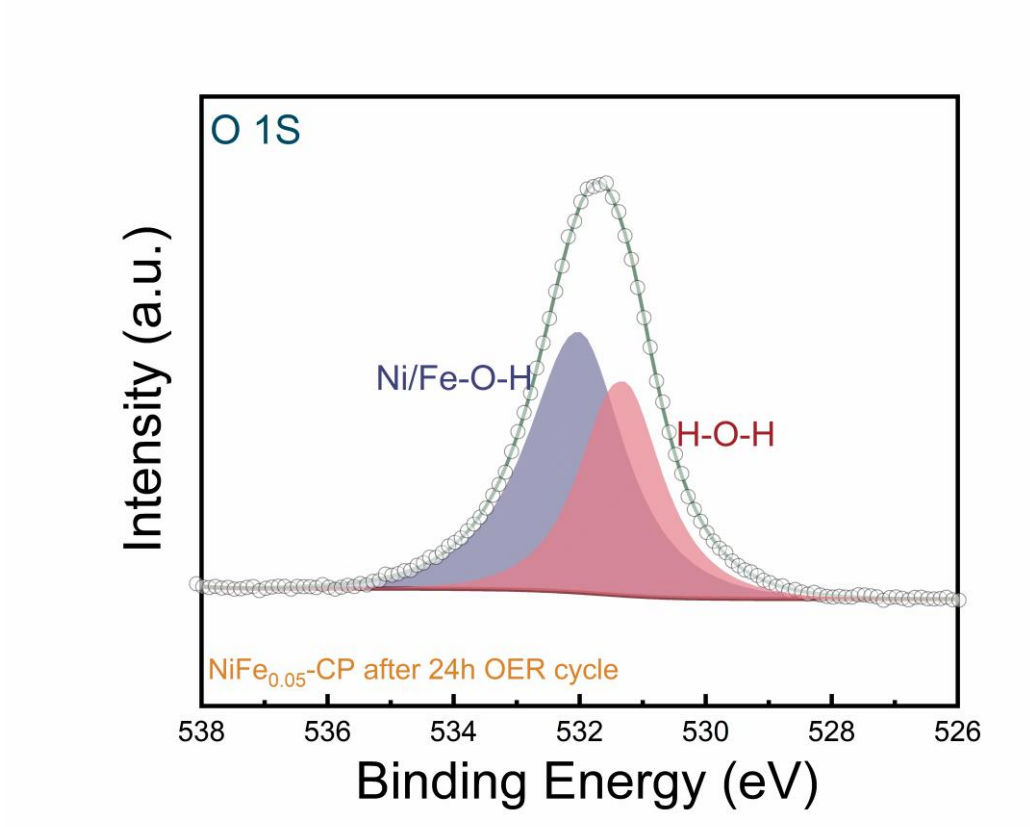

Fig. S13 High-resolution O 1S XPS spectra of $NiFe_{0.05}$-N-CP after24h OER cycling.

Table S1 OER performance of NiFe-N-CP and other representative reported non-precious metal electrocatalysts in similar alkaline media.

Electrocatalysts	Current density ($mA\ cm^{-2}$)	Overpotential (mV)	References
$NiFe_{0.05}$-N-CP	**10** **100**	**238** **320**	**This work**
$NiFe_{0.1}$-N-CP	10 100	264 340	This work
$NiFe_{0.01}$-N-CP	10 100	261 348	This work
$NiFe_{0.2}$-N-CP	10 100	275 349	This work
Ni-N-CP	10 100	280 416	This work
Fe-N-CP	10	427	This work
$Fe_{0.052}$Ni-POMo	10	255.3	*Adv. Funct. Mater.,* **2021**[1]
CoFe LDH-S	10	270	*Chem. Commun*., **2021**[2]
FeCoNi-NS	10 100	251 366	*Chem. Commun*., **2019**[3]
Ni-N-C	10	331	*Nat. Catal*., **2018**[4]
Tannin-NiFe	10	290	*Angew. Chem. Inter. Ed*., **2019**[5]
G-$Ni_{0.5}Fe_{0.5}$	10	280	*Adv. Energy Mater*.,**2020**[6]
HCM@Ni-N	10	304	*Adv. Mater*. **2019**[7]
NiFe-LDH-UF	10 100	254 320	*Adv. Energy Mater*. **2018**[8]
FeNi@FeNiB-700	10	272	*J. Mater. Chem. A* **2019**[9]
$NiCo_2S_4$	10	337	*Green Chem.*, **2017**[10]
$LaFe_XNi_{1-X}O_3$	10	302	*Angew. Chem. Int. Ed*., **2019**[11]
NiCoFeB	10	284	*Small*, **2019**[12]
CoS_x/Ni_3S_2	10 100	280 373	*ACS Appl. Mater. Interfaces,* **2018**[13]
Ni_3S_2	10 100	296 370	*J. Mater. Chem. A* **2019**[14]

Fe/Fe_3C-MC	10	320	*Angew. Chem. Int. Ed*., **2021**[15]
$La_{0.5}Sr_{0.5}Co_{0.8}Fe_{0.2}O_3$	10	304	*Nanoscale*, **2020**[16]
CoOOH	10	291	*ACS Sustainable Chem. Eng.,* **2019**[17]

3. References

1. X. Liu, F. Xia, R. Guo, M. Huang, J. Meng, J. Wu and L. Mai, *Adv. Funct. Mater.,* 2021, **31**, 2101792.
2. Y. Zhou, J. Hu, D. Li and Q. Gao, *Chem. Commun*., 2021,**57**, 7653-7656.
3. J. Jiang, L. Chang, W. Zhao, Q. Tian and Q. Xu, *Chem. Commun*., 2019,**55**, 10174-10177.
4. H. Fei, J. Dong, Y. Feng, C. S. Allen, C. Wan, B. Volosskiy, M. Li, Z. Zhao, Y. Wang, H. Sun, P. An, W. Chen, Z. Guo, C. Lee, D. Chen, I. Sharir, M. Liu, T. Hu, Y. Li, A. I. Kirkland, X. Duan and Y. Huang, *Nat. Catal*., 2018, **1**, 63-72.
5. Y. Shi, Y. Yu, Y. Liang, Y. Du and B. Zhang, *Angew. Chem. Inter. Ed*., 2019, **58**, 3769-3773.
6. H. Khani, N. S. Grundish, D. O. Wipf and J. B. Goodenough, *Adv. Energy Mater*., 2020, 10, 1903215.
7. H. Zhang, Y. Liu, T. Chen, J. Zhang, J. Zhang and X. Lou, *Adv. Mater*., 2019, **31**, 1904548.
8. Y. Zhao, X. Zhang, X. Jia, G. I. N. Waterhouse, R. Shi, X. Zhang, F. Zhan, Y. Tao, L. -Z. Wu, C.- H. Tung, D. O'Hare and T. Zhang, *Adv. Energy Mater*., 2018, **8**, 1703585.
9. H. Yuan, S. Wang, X. Gu, B. Tang, J. Li and X. Wang, *J. Mater. Chem. A,* 2019, **7**, 19554-19564.
10. J. Jiang, C. Yan, X. Zhao, H. Luo, Z. Xue and T. Mu*, Green Chem.*, 2017, **19**, 3023-3031.
11. H. P. Wang, J. Wang, Y. C. Pi, Q. Shao, Y. Tan and X. Huang, *Angew. Chem. Int. Ed*., 2019, **58**, 2316-2320.
12. Y. Li, B. Huang, Y. Sun, M. Luo, Y. Yang, Y. Qin, L. Wang, C. Li, F. Lv, W. Zhang and S. Guo, *Small,* 2019, **15**, 1804214
13. S. Shit, S. Chhetri, W. Jang, N. C. Murmu, H. Koo, P. Samanta and T. Kuila, *ACS Appl. Mater. Interfaces,* 2018, **10**, 27712-27722
14. L. Li, C. Sun, B. Shang, Q. Li, J. Lei, N. Li and F. Pan, *J. Mater. Chem. A,* 2019, **7**, 18003-18011.
15. X. Liang, J. Xiao, W. Weng and W. Xiao, *Angew. Chem. Int. Ed*., 2021, **60**, 2120-2124.
16. K. Rong, J. Wei, L. Huang, Y. Fang and S. Dong, *Nanoscale*, 2020, **12**, 20719-20725.
17. S. Liu, C. Zhang, B. Zhang, Z. Li and J. Hao, *ACS Sustainable Chem. Eng.*, 2019, **7**, 8964-8971